20. EXTREME RAINFALL (R20MM, RX5DAY) IN YANGTZE–HUAI, CHINA, IN JUNE–JULY 2016: THE ROLE OF ENSO AND ANTHROPOGENIC CLIMATE CHANGE

Qiaohong Sun and Chiyuan Miao

Both the 2015/16 strong El Niño and anthropogenic factors contributed to the June–July 2016 extreme precipitation (R20mm, RX5day) in Yangtze–Huai, China. Combined, they increased the risk of the event tenfold.

Introduction. In June–July 2016, the Yangtze–Huai region (27.5°–35°N, 107.5°–123°E) in China experienced a deluge of extreme rainfall, especially in the middle and lower reaches of the Yangtze River Basin (Fig. ES20.1a). The extreme rainfall caused widespread severe flooding, waterlogging, and landslides in the Yangtze–Huai region.

We examined changes in the characteristics of rainfall for the June–July period, including the number of days with very heavy precipitation (daily precipitation ≥ 20 mm; R20mm) and the maximum 5-day precipitation amount (RX5day). In this study, we estimated the probability that the changes in extreme rainfall were due to El Niño or to anthropogenic climate change.

Data and methods. We used observed daily precipitation data for the period 1957–2016, obtained from the National Meteorological Information Center of the China Meteorological Administration. The dataset is constructed from over 2400 station observations across China at a resolution of 0.5° × 0.5° (Shen et al. 2010). We calculated R20mm and RX5day (Sillmann et al. 2013) to estimate the characteristics of extreme precipitation in June–July. We conducted a lag–lead correlation between the June–July extreme precipitation and the December–February (DJF) ENSO index during the preceding winter. The DJF oceanic Niño index (ONI, 3-month running mean of ERSST.v4 SST anomalies in the Niño-3.4 region), based on centered 30-year base periods updated every 5 years, was used as an indicator of the ENSO.

AFFILIATIONS: Sun and Miao—State Key Laboratory of Earth Surface Processes and Resource Ecology, Geographical Science, Beijing Normal University, Beijing, China

DOI:10.1175/BAMS-D-17-0091.1

A supplement to this article is available online (10.1175/BAMS-D-17-0091.2)

Simulations from six climate models involved in phase 5 of the Coupled Model Intercomparison Project (CMIP5; Taylor et al. 2012) that adequately capture climate variability in the Yangtze–Huai region were used to attribute the June–July extreme precipitation over Yangtze–Huai (see Table ES20.1). We used simulations for the period 1912–2005 with natural forcing and all forcings. We obtained the simulated RX5day and R20mm data from the Canadian Centre for Climate Modelling and Analysis (www.cccma.ec.gc.ca/data/climdex/index.shtml). Data from NCEP/NCAR Reanalysis 1 were used to depict large-scale atmospheric circulation. We used several statistical techniques to assess the severity and causes of the extreme precipitation:

1) To estimate the univariate return period, we used the generalized extreme value (GEV) distribution for parametric fitting. We used the Kolmogorov–Smirnov (K–S) goodness-of-fit test to verify the distribution (Wilks 2006). The return periods (R) for RX5day and R20mm were estimated from the GEV distribution and defined as $R = 1 / [1 - F(x)]$, where F(x) is the cumulative probability of June–July RX5day or R20mm in 2016. Then, after using the Akaike Information Criterion (AIC; Akaike 1974) to identify the most appropriate copula function (smallest AIC), the T-copula function was used to estimate the probability of concurrence of high RX5day and R20mm.

2) To assess the influence of the 2015/16 El Niño on the 2016 extreme precipitation, we used the nonstationary GEV distribution with the ENSO index in the preceding winter as a covariate. The location parameter of the GEV distribution was linearly regressed to the DJF ENSO index (Sun et al. 2017; Zhang et al. 2010). Then, the probability ratios ($PR = P_1/P_2$) were used to estimate the influence of ENSO. P_1 and P_2 represent the probabilities of exceeding the June–July RX5day threshold in two different scenarios. P_1

was estimated from the GEV distribution with the parameter fit to the winter 2015/16 ENSO index; P_2 was calculated from the GEV distribution fitted to the ENSO index from the neutral years.

3) To quantify the human-induced changes in the odds of extreme events, we employed the fraction of attributable risk (FAR = $1 - P_2/P_1$) and the corresponding probability ratios (Fischer and Knutti 2015; Stott et al. 2005). We estimated the anthropogenic influence by setting P_1 to be the probability of exceeding the 2016 RX5day in the all-forcings scenarios, with P_2 being the equivalent for the natural-forcing scenarios. To estimate the influence of El Niño conditions during the preceding winter on the June–July extreme precipitation, we calculated the probability ratio (*PR*) with P_1 from the El Niño all-forcings simulations and P_2 from the neutral all-forcings simulations. The sample method (90% of samples were randomly selected for each time) was performed 1000 times per period to estimate the *PR* uncertainty.

Results A. Observed 2016 June–July extreme rainfall in historical context. The regional averages for the 2016 June–July RX5day (127.04 mm) and R20mm (7.91 days) were the third highest since records began in 1957, with 45.1% and 47. 9% growth relative to the baseline period (1961–90), respectively (Fig. 20.1a). 2016–like RX5day and R20mm events occur in the present climate in the Yangtze–Huai region approximately every 116 years (95% confidence level: 45–2947 years) and 51 years (95% confidence level: 25–234 years), respectively, but the concurrency of the two events was close to being a 1-in-181-year event (Fig. 20.1a). The maximum changes in RX5day were concentrated in the middle and lower reaches of the Yangtze River Basin, where there were positive anomalies greater than 100% (Fig. 20.1b). More regions were affected by severe precipitation in 2016 compared with the baseline period, as demonstrated by the distinct rightward shift in the 2016 histogram for RX5day (Fig. 20.1b). Successive days of heavy precipitation were mainly concentrated in late June and early July. The water levels in five main hydrological stations surpassed the alert level for long durations, triggering widespread, severe flooding in the middle and lower reaches of the Yangtze River Basin (Fig. ES20.2).

Results B. Attribution to El Niño and anthropogenic influences. The 2015/16 El Niño was one of the strongest on record, comparable to the 1972/73 event (L'Heureux et al. 2017). The ENSO index during the preceding winter was significantly correlated ($p < 0.05$) with the June–July extreme precipitation and flooding in the Yangtze–Huai region (Fig. 20.1c), and the correlation map has field significance ($p < 0.05$) as suggested by the field significance test (Livezey and Chen 1983; Fig. ES20.1b). The risk of occurrence of the 2016 extreme precipitation event was increased by the preceding winter El Niño, with a 1.5- to 4-fold increase in risks relative to preceding neutral conditions for most areas in the Yangtze–Huai region (Fig. 20.1d). Comparing precipitation extremes between the preceding El Niño and neutral seasons in the all-forcings simulations, we found that about 72% of the risk of the June–July 2016 RX5day could be attributed to the influence of El Niño, indicating that the El Niño event produced a greater than threefold increase in the likelihood of the extreme precipitation event (Figs. ES20.2a,b). The western Pacific subtropical high (WPSH) generally shifts southward and has a westward extension during El Niño decay (Huang and Wu 1989; Wang et al. 2000), which is conducive to water-vapor transmission to the Yangtze–Huai region and the induction of persistent heavy precipitation in the Yangtze River Basin (Figs. 20.1e,f). The circulation systems in June–July of 1998 and 2016 were characterized by a stronger than normal WPSH with its high ridge extending more westward. The high ridge of the WPSH in 2016 was slightly eastward compared to that in 1998 owing to some inconsistences of sea surface temperature patterns (L'Heureux et al. 2017); however, the intensity of the WPSH in 2016 was slightly stronger than that in 1998. An anomalous anticyclone dominated over the northwestern Pacific in the lower troposphere and induced intensified water vapor transport from the western Pacific to the Yangtze–Huai region (Yuan et al. 2017); this transport was linked to the occurrence of extreme precipitation.

We compared the likelihood of occurrence of the 2016 June–July RX5day event in different CMIP5 experiments. When the 2016 June–July RX5day was marked as the threshold, precipitation extremes like those experienced during June–July 2016 in the Yangtze–Huai region were 35% more likely because of anthropogenic climate change. This is equivalent to an approximately 1.5-fold (5%–95% uncertainty range: 0.6–4.7) increase in the probability of occurrence owing to anthropogenic influences. The compound effects of both anthropogenic climate change and the preceding strong El Niño can explain 91% (5%–95% uncertainty range: 66%–99%) of the risk of such event conditional on the preceding winter El Niño state between all-forcings and natural-forcing

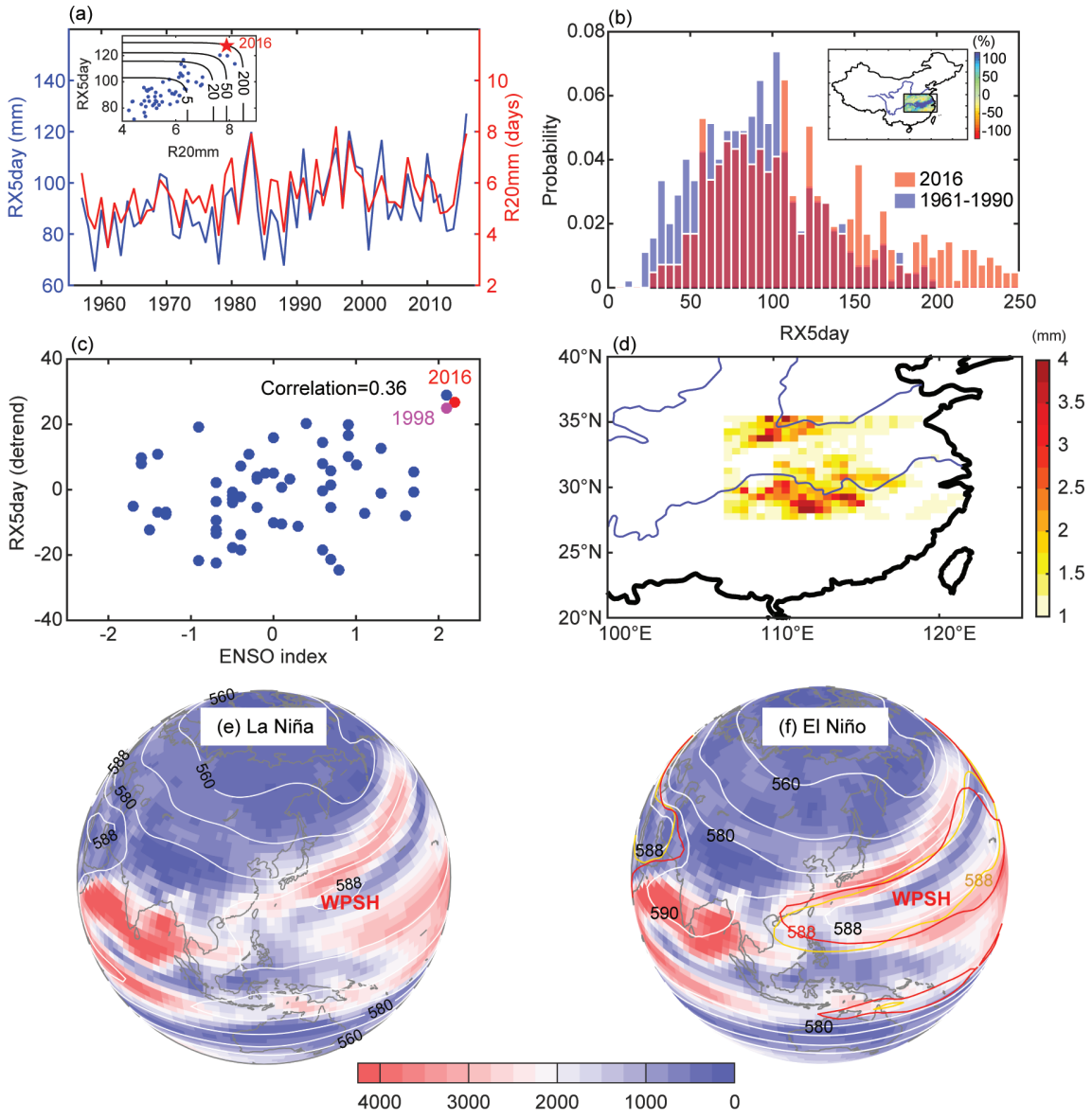

Fig. 20.1. (a) Time series for Jun–Jul RX5day (blue) and R20mm (red) over the Yangtze–Huai region (area in black box in Fig. ES20.1a) for the period 1957–2016. Embedded figure shows bivariate return periods for concurrent RX5day and R20mm. (b) Standardized histograms of RX5day values over Yangtze–Huai region in 2016 (red) and in baseline period (1961–90; blue). Embedded figure shows spatial distribution of percentage change (%) in Jun–Jul RX5day in 2016 relative to mean RX5day during baseline period (1961–90). (c) ENSO index during preceding winter and area-averaged Jun–Jul RX5day were significantly correlated at 95% confidence level (r = 0.365). (d) Spatial distribution of probability ratio, with preceding winter ENSO index as covariate, representing difference in probability of 2016 RX5day event occurring during decaying El Niño conditions versus during neutral conditions. (e),(f) Mean Jun–Jul integrated water-vapor flux g m^{-1} s^{-1} of layer from surface to 300 hPa and 500 hPa geopotential height on (white contours) for (e) five strongest La Niña years and (f) five strongest El Niño years. Red and orange contour lines in (f) are for 588 dagpm in Jun–Jul 2016 and 1998, respectively.

simulations. That is, anthropogenic climate change and El Niño together resulted in a tenfold increase in the risk of this extreme event (Fig. 20.2b).

Conclusions. Model and observational analyses showed that the extreme precipitation event that occurred in June–July 2016 in the Yangtze–Huai region of China, featuring high intensity and frequency of precipitation, was strongly correlated with the preceding 2015/16 El Niño conditions and with anthropogenic factors. The El Niño conditions during the preceding winter strongly increased the probability of summer

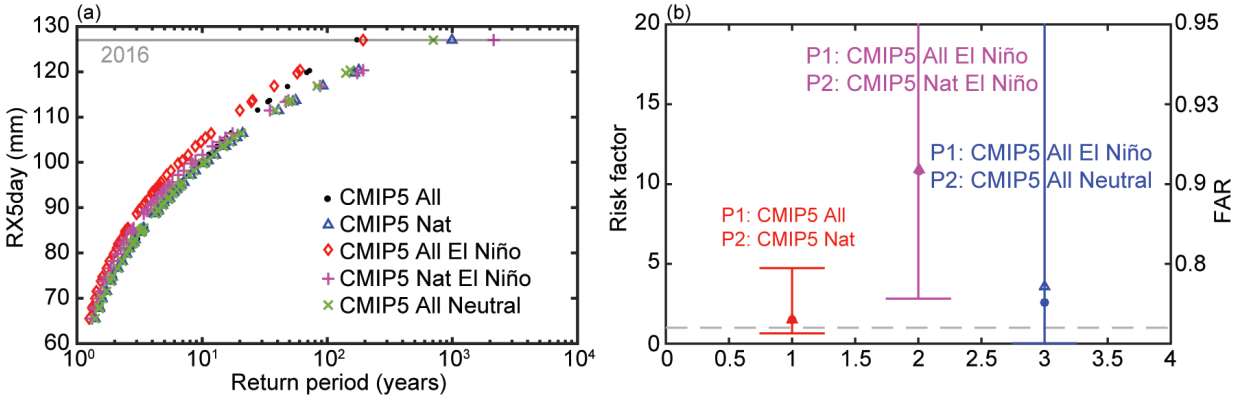

Fig. 20.2. (a) Return period plots for Jun–Jul RX5day under various modeling scenarios. Horizontal line represents 2016 RX5day. (b) Corresponding probability ratios and FAR calculated using different scenario combinations for P_1 and P_2, as indicated. Estimates of probability ratios were calculated using a bootstrapping approach (resampling the distributions 1000 times with replacement); bars show the interquartile range (5th–95th percentiles); dots and triangles show median values and best estimates, respectively.

extreme precipitation over the Yangtze–Huai region via an enhancement and westward extension of the WPSH. The models showed a 35% contribution of anthropogenic factors to the 2016 extreme precipitation. Together, anthropogenic climate change and El Niño may result in a tenfold increase in the risk of occurrence of this extreme event. The frequency of extreme El Niño events are projected to increase with a warming climate (Cai et al. 2014), which may induce more frequent and more severe episodes of extreme precipitation in the future.

ACKNOWLEDGMENTS. This research was supported by the National Natural Science Foundation of China (No. 41622101; No. 91547118), and the State Key Laboratory of Earth Surface Processes and Resource Ecology. We acknowledge the World Climate Research Programme's Working Group on Coupled Modeling, which is responsible for CMIP. We are grateful to the National Meteorological Information Center of the China Meteorological Administration for archiving the observed climate data.

REFERENCES

Akaike, H., 1974: A new look at the statistical model identification. *IEEE Trans. Automat. Contr.*, **19**, 716–723, doi: 10.1109/TAC.1974.1100705.

Cai, W., and Coauthors, 2014: Increasing frequency of extreme El Niño events due to greenhouse warming. *Nat. Climate Change*, **4**, 111–116, doi:10.1038/nclimate2100.

Fischer, E. M., and R. Knutti, 2015: Anthropogenic contribution to global occurrence of heavy-precipitation and high-temperature extremes. *Nat. Climate Change*, **5**, 560–564, doi:10.1038/nclimate2617 .

Huang, R., and Y. Wu, 1989: The influence of ENSO on the summer climate change in China and its mechanism. *Adv. Atmos. Sci.*, **6**, 21–32, doi:10.1007/BF02656915.

L'Heureux, M., and Coauthors, 2017: Observing and predicting the 2015/16 El Niño. *Bull. Amer. Meteor. Soc.*, **98**, 1363–1382, doi:10.1175/BAMS-D-16-0009.1

Livezey, R. E., and W. Chen, 1983: Statistical field significance and its determination by Monte Carlo techniques. *Mon. Wea. Rev.*, **111**, 46–59, doi:10.1175/1520-0493(1983)111<0046:SFSAID>2.0.CO;2.

Shen, Y., A. Xiong, Y. Wang, and P. Xie, 2010: Performance of high-resolution satellite precipitation products over China. *J. Geophys. Res.*, **115**, D02114, doi:10.1029/2009JD012097.

Sillmann, J., V. V. Kharin, X. Zhang, F. W. Zwiers, and D. Bronaugh, 2013: Climate extremes indices in the CMIP5 multimodel ensemble: Part 1. Model evaluation in the present climate. *J. Geophys. Res.*, **118**, 1716–1733, doi:10.1002/jgrd.50203.

Stott, P. A., D. A. Stone, and M. R. Allen, 2005: Human contribution to the European heatwave of 2003. *Nature*, **436**, 610–614, doi:10.1038/nature03089.

Sun, Q., C. Miao, Y. Qiao, and Q. Duan, 2017: The non-stationary impact of local temperature changes and ENSO on extreme precipitation at the global scale. *Climate Dyn.*, online, doi:10.1007/s00382-017-3586-0.

Taylor, K. E., R. J. Stouffer, and G. A. Meehl, 2012: An overview of CMIP5 and the experiment design. *Bull. Amer. Meteor. Soc.*, **93**, 485–498, doi:10.1175/BAMS-D-11-00094.1.

Wang, B., R. G. Wu, and X. H. Fu, 2000: Pacific-East Asian teleconnection: How does ENSO affect East Asian climate? *J. Climate*, **13**, 1517–1536, doi:10.1175/1520-0442(2000)013<1517:PEATHD>2.0.CO;2.

Wilks, D. S., 2006: *Statistical Methods in the Atmospheric Sciences*. 2nd ed. International Geophysics Series, Vol. 91, Elsevier, 627 pp.

Yuan, Y., H. Gao, W. Li, Y. Liu, L. Chen, B. Zhou, and Y. Ding, 2017: The 2016 summer floods in China and associated physical mechanisms: A comparison with 1998. *J. Meteor. Res.*, **31**, 261–277, doi:10.1007/s13351-017-6192-5.

Zhang, X., J. Wang, F. W. Zwiers, and P. Ya. Groisman, 2010: The influence of large-scale climate variability on winter maximum daily precipitation over North America. *J. Climate*, **23**, 2902–2915, doi:10.1175/2010JCLI3249.1.